

Heterogeneous photocatalytic degradation of anionic dye on polyaniline/microcrystalline cellulose composite

Soumya Noria Benaouda¹ · Hanane Chaker^{1,2} · Fatiha Abidallah³ · Cherifa Bachir^{1,4} · Hashem Tawheed⁵ · Peter G. Weidler⁵ · Abdelkader Bengueddach⁴ · Jesús Canales-Vázquez⁶ · Rachida Hamacha⁴

Abstract

The development of novel polymeric composites, especially those based on conductive polymers has attracted a considerable attention due to their applications in a wide range of fields. This study focuses on one of these biocomposites based on polyaniline Pani and a biopolymer (microcrystalline cellulose MCC), synthesized by in-situ polymerization of aniline using ammonium persulfate (APS) as oxidant at room temperature. Firstly, different amounts of MCC were dispersed in HCl solution with aniline monomer under stirring. Then a mixture of APS/HCl solution was introduced into the first aniline-MCC-HCl mixture. The obtained materials as well as Pani and MCC were characterized using powder X-ray diffraction (XRD), Argon adsorption-desorption (BET/DFT), thermal analysis, fourier transform infrared spectroscopy (FTIR), scanning electron microscopy (SEM), and transmission electron microscopy (TEM). Thus, a correlation between interesting structural/textural/morphological data of these materials will be established. The results confirm the formation of Polyaniline-MCC composite under well determined conditions which has a more compact homogeneous morphology and a higher thermal stability than those of Pani and MCC. Furthermore, these materials are used for the catalytic degradation of toxic anionic dye namely Methyl Orange (MO) from aqueous media under UV light irradiation. The optimum values were 0.1 g L⁻¹ of photocatalyst, 30 ppm of MO solution, and pH solution of 5.6, which allowed reaching 97% within 70 min with high stability after four continuous runs. The photodegradation kinetics of MO onto composite followed the pseudo-first order model.

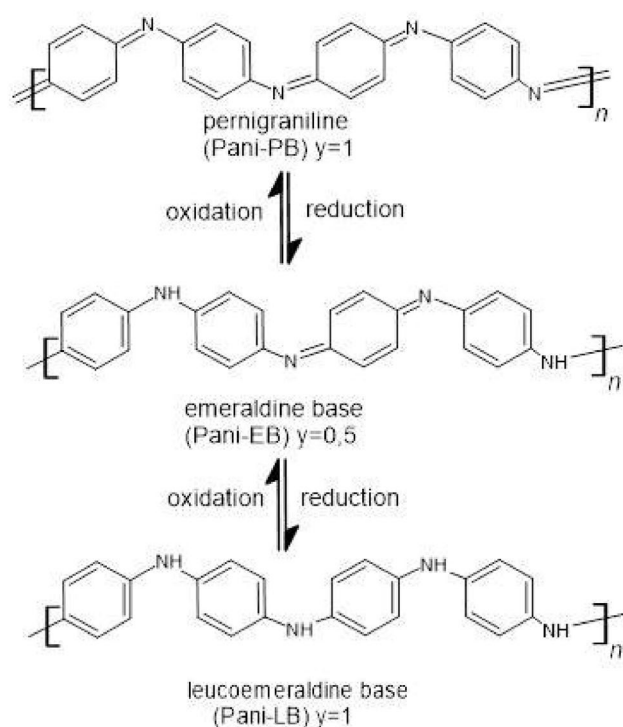
Keywords Biocomposite · Polyaniline · Microcrystalline cellulose · In-situ polymerization · Photocatalysis · Methyl orange

1 Introduction

The current trend of developing new materials from renewable resources exhibits an alternative sources to petroleum and environmental concern in the materials science and technology fields [1, 2]. MCC-based polymer composites have drawn a lot of concern due to their several advantages, such as low cost, availability, light weight, interesting mechanical properties, and nontoxic properties [3]. The use of conductive polymers has many advantages, such as ease of synthesis, low cost, good environmental stability, and the ability to be electrically switched between its conductive and resistive states [4]. Among a large spectrum of semiconductors, Pani is a promising candidate for technological applications in various areas like sensors [5], super-capacitors [6], corrosion inhibitors [7], and EMI shielding [8]. Thus, Pani is regarded as a regenerable adsorbent/reductant for detoxification of Cr(VI)-contaminated effluents [9–13]. Pani and its composites can be used as adsorbents to remove anionic

✉ Soumya Noria Benaouda
soum46@yahoo.fr

- ¹ Laboratoire de Chimie Appliquée, Université d'Aïn-Témouchent, Route Sidi Bel Abbes BP 284, 46000 AïnTémouchent, Algeria
- ² Laboratoire de Catalyse Et Synthèse en Chimie Organique, Université de Tlemcen, BP 119, 13000 Tlemcen, Algeria
- ³ Département de Génie Des Matériaux, Faculté de Chimie, Université Des Sciences Et de La Technologie Mohamed Boudiaf, 31000 Oran, Algeria
- ⁴ Laboratoire de Chimie Des Matériaux, Université Oran 1 Ahmed Ben Bella, BP1524 El-Mnaouer, 31000 Oran, Algeria
- ⁵ Institute of Functional Interfaces, Karlsruher Institut Für Technologie KIT, Hermann-von-Helmholtz-Platz 1, 76344 Eggenstein-Leopoldshafen, Germany
- ⁶ Materials for Energy and 3D Printing Laboratory, University of Castilla-La Mancha, Calle Investigación 1, Edif. 3, 02071 Albacete, Spain



Scheme 1 Different forms of polyaniline bases [21]

and cationic dyes due to the presence of large amounts of amine and imine functional groups in the polymer chains [14–18]. However, Pani has some disadvantages such as its low dispersibility and solubility in most solvents [19]. Pani semiconductor exists in various forms based on its oxidation level: the fully oxidized pernigraniline base, half-oxidized emeraldine base and fully reduced leucoemeraldine base (Scheme 1), although, emeraldine, is the most stable and conductive. Emeraldine Base (EB) which has electrical insulator properties and can be converted into Emeraldine Salt (ES), which owns conductive properties by doping EB with protonic acid [20].

Known as an available natural biopolymer, Microcrystalline cellulose (MCC) has a high potential to be used in several fields such as a water retainer and suspension stabilizer, in the pharmaceutical, cosmetics, food industries, and particularly as reinforcement in the development of composites [22]. MCC has recently gained more interest owing as it is renewable, non-toxicity, economic low cost, biodegradable, biocompatible and exhibits high excellent mechanical properties, and high surface area and biocompatibility [23].

Some 80 percent of the world's wastewater is dumped largely untreated back into the environment, polluting rivers, lakes, and oceans [24]. Thus, for the treatment of wastewater to remove organic compounds, such as organic pesticides, and azo dyes, the application of an advanced oxidation process (AOPs) is a promising way to perform

the mineralization of this type of substances. The principal mechanism of AOPs function is the generation of highly reactive free radicals such as hydroxyl radical (OH^\cdot), superoxide radicals ($\text{O}_2^{\cdot-}$) [25, 26]. Among many AOPs, photocatalysis can be very easily carried out under ambient conditions and leads to the total mineralization of organic carbon to CO_2 and H_2O [27–32].

In photocatalytic processes, a semiconductor photocatalyst is activated with light irradiation as activation energy to in situ generate reactive radicals, allowing the complete degradation of the pollutants [33–39]. Among them, most studies focused on using metal oxide nanoparticles such as catalysts [40–46]. However, the application of metal oxide nanoparticles requires loading them on supporting materials, which is difficult due to the low surface activity of inorganic nanoparticles, which limited its application on a large scale [47, 48].

Furthermore, Pani and their composites are considered as a potential photocatalytic material to remove waste organic dyes during recent years [49–53]. Up to now, these materials are not completely well investigated. Thus the aim of this work is the synthesis, characterization and application of Pani and Pani/MCC composites. Non-covalent interactions were built between MCC and Pani in the acidic medium which that helped to construct the composite, and the effect of this interaction will be studied. The structural/textural and morphological features as well as thermal stability of materials were investigated through X-ray diffraction (XRD), argon adsorption isotherms at 87 K, Fourier transform infrared spectroscopy (FTIR), scanning electronic microscopy (SEM), transmission electron microscopy (TEM) and thermogravimetric analysis (TGA). A combination of interesting structural/textural data of materials with their properties will be studied using different characterization methods with particular, emphasis in particular, on the correlation between hydrophilicity and conductive activity in the homogeneous union of neat materials. The photocatalytic activity of these materials will be tested via the methyl orange photodegradation under UV–Visible light irradiation. The principle of heterogeneous photocatalysis is based on the promotion of electrons from the valence band to the conduction band through the illumination of a semiconductor with photons of energy equal to or greater than its the gap energy and an effective way to promote charge (e^-/h^+) separation for potential photocatalytic applications [54, 55].

Based on the knowledge acquired from our previous work where several experimental parameters were tested [27, 28, 48], we focused on these values. Our main goal in this study is rather to test a new catalyst (composite based conductive polymer). Pani is a valid catalyst for the photocatalytic degradation of MO, as it exists in various forms based on its oxidation level which can facilitate electron transfer and thus improve the photoactivity. However, its poor dispersion led

to much slower degradation rates, resulting from the poor accessibility of dye of dye molecules to the catalyst. Moreover, the MCC will increase the dispersibility of Pani particles in aqueous solution, which will result in better catalytic activity comparing to neat Pani [47]. Another important goal of this work is the application of the DFT method rather than the BJH in the pore analysis of polymers and biopolymers.

2 Experimental section

2.1 Materials and methods

Analytical grade aniline (C_6H_7N), was purchased from Biochem-chempharama and distilled before use. Fine powder microcrystalline cellulose (MCC), hydrochloric acid (HCl) (37%), ethanol (C_2H_5OH) (96%), methyl orange ($C_{14}H_{14}N_3NaO_3S$, 99.99%) and ammonium persulfate (APS) ($(NH_4)_2S_2O_8$) were purchased from Sigma-Aldrich.

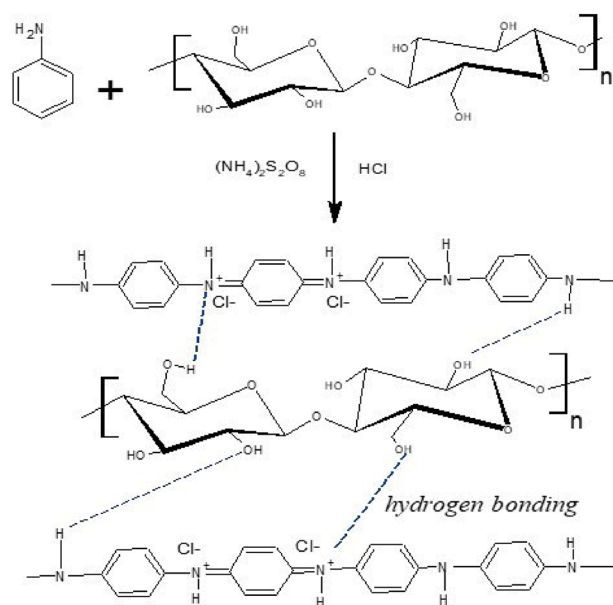
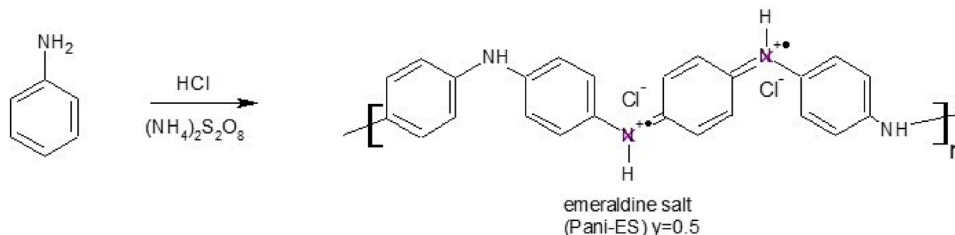
2.2 Synthesis of doped pani

Polyaniline was synthesized by oxidative polymerization of aniline monomer using ammonium persulfate (APS) as oxidant at room temperature (Scheme. 2). In this work the oxidant/monomer molar ratio was $n_{ox}/n_{an}=1$. Firstly, amount of aniline was dispersed in 30 mL of 1 M HCl solution under stirring for 1 h, then a mixture of APS/HCl solution was introduced dropwise into the first aniline-HCl mixture and stirred for further 24 h. The greenish black precipitate was then filtered, washed with distilled water and ethanol. The formed solid was dried overnight at 60 °C.

2.3 Synthesis of pani/MCC composite

The composite was synthesized by in situ oxidative polymerization of aniline monomer using ammonium persulfate (APS) as oxidant at room temperature (Scheme 3). In this case, the oxidant/monomer molar ratio was $n_{ox}/n_{an}=1$ as well. Firstly, amount of MCC was dispersed in 30 mL of 1 M HCl solution containing 1 g of aniline under by stirring for 1 h. Then a mixture of APS/HCl solution was introduced dropwise into the first aniline-MCC-HCl mixture and stirred for further 24 h. The composites obtained were filtered,

Scheme 2 Synthesis of pani-ES



Scheme 3 Synthesis of Pani-ES/MCC composite and possible interactions between cellulose and Pani (emeraldine salt)

washed with distilled/ethanol and dried at 60 °C overnight. To evaluate the effect impact of the MCC content in the properties of the composite, different wt % MCC loading were prepared. The prepared samples were designated as Pani: pure polyaniline; composite as Pani/MCC X%.

2.4 Characterization methods

X-ray diffraction (XRD) was carried out on a Bruker AXS D8 advance diffractometer working with $CuK\alpha$ radiation ($\lambda=1.54056 \text{ \AA}$) equipped with a Lynxeye Trade Mark (TM) position sensitive stripe detector. Diffractograms were recorded over the range $2-70^\circ 2\theta$ (step size $0.02^\circ 2\theta$, step time 4 s). Textural properties were determined by argon sorption-desorption measurements. Argon adsorption-desorption measurements were performed at 87 K using a Quantachrome Autosorb-IMP instrument in the relative pressure range P/P_0 from 10^{-5} to 1. The samples were outgassed overnight at 373 K prior to adsorption analysis. Specific surface areas, SSA, were calculated according to the Brunauer-Emmett-Teller (BET) method [56, 57]. The non- local density functional theory (NLDFT)

was used to calculate the total pore volume V_p . The NLDFT differential pore volume distribution curves of all materials were also illustrated. The Ar adsorption–desorption isotherms have been also established, in order to get information on the forms of the isotherms and their hysteresis loop which are related to the pore nature existing in their structure [58, 59]. The analysis of the surface morphology and particle size and distribution of the materials was carried out using environmental scanning electron microscopy ESEM (Philips ESEM XL 30 FEG) and Transmission electron microscopy (TEM, 2100 JEOL operating at 200 kV).

The Fourier transform infrared spectroscopy (FTIR) was operated on a Fourier transforms infrared Spectrum Bruker in the range between 4000 and 400 cm^{-1} with a resolution of 4 cm^{-1} , using the KBr pellet. Thermogravimetric analysis and its derivative thermogravimetric (TGA/DTG) of materials were performed in a thermo-gravimetric balance TGA LABSYS Evo under air atmosphere in the 36–1100 $^{\circ}\text{C}$ temperature range. To study the optical properties of catalysts, The UV–Vis reflectance diffuse (RD/UV–Vis) spectra were recorded on a Varian Cary 100 Scan UV–Vis Spectrophotometer equipped with an integrating sphere accessory in the diffuse reflectance mode (R). It is important to highlight that the inorganic compound of Barium sulfate (BaSO_4) was used as a reference material.

2.5 Photocatalytic activity

The photocatalytic activity of Pani and composite based on Pani was tested in photodegradation of both cationic dye methylene blue and anionic dye methyl orange. Due to the selectivity of our catalytic system via anionic dye, methyl orange has been used for further investigations.

Photodecolorization experiments were carried out under UV–Vis lamp photoreactor ($\lambda = 360 \text{ nm}$, $I = 20 \text{ mW/cm}^2$). A magnetic stirrer of the suspension was used to assure a good mixing. In order to control the temperature of the system a water jacket was placed close to the photoreactor, thus, the photodegradation reaction was carried out at room temperature ($25 \pm 3 \text{ }^{\circ}\text{C}$) using 0.1 g L^{-1} of the prepared solids in 100 mL of 30 ppm dye solution. Firstly, the suspension was kept under stirring for 30 min in darkness for the adsorption–desorption equilibrium. Then, the suspension was irradiated and aliquots were taken every 15 min. The aliquots absorbance was measured at $\lambda = 463 \text{ nm}$ using a “SPECORD” UV spectrophotometer.

The photodegradation yield has been determined using the following equation:

$$\text{Conversion (\%)} = \frac{C_0 - C_{\text{residue}}}{C_0} * 100 \quad (1)$$

where C_0 is the dye initial concentration and C_{residue} is the concentration of suspension at time t .

3 Results and discussions

3.1 Characterization of materials

3.1.1 X-ray diffraction

The ordered arrangement of polymer chains in the crystalline phase can be detected via X-ray diffraction study. The XRD patterns of pure Pani, MCC and Pani/MCC composites are presented in Fig. 1. The pattern of pure Pani exhibits two diffraction peaks at $2\theta = 20.5^{\circ}$ and 25.2° assigned to the (100) and (110) planes respectively [60], which are related to the repetition of the benzoid and quinoid rings in the Pani chains [61, 62]; These reflections confirm that polyaniline was in the form of emeraldine salt [63]. There also appear other two weak peaks centered at 9.2° and 15.3° that could be ascribed to (001) and (010), which were indicative are usually associated to monoclinic $P2_1$ space group [60, 64]. This is typically can be explained by the fact that in terms of the insertion of Cl^- anions between polymer chains adds Coulomb force, which makes the structure more rigid and favours the crystalline state [60]. In this case it is interesting to note that by doping with HCl, small crystalline regions are formed in emeraldine base form [60]. The XRD pattern of MCC shows a typical pattern for cellulose I, i.e. the highest intensity peak appears at $2\theta = 23.09^{\circ}$, and two weak peaks at $2\theta = 15.37^{\circ}$ and 17.92° correspond to the (200), (1–10) and (110) reflexions, respectively. Another small peak appears at $2\theta = 34.08^{\circ}$ that can be ascribed to the (040) reflexion [65]. On the other hand, the XRD patterns of the Pani/MCC composites exhibited the highest intensity peak at 25.2° and shows the presence of the same peaks characteristic of the

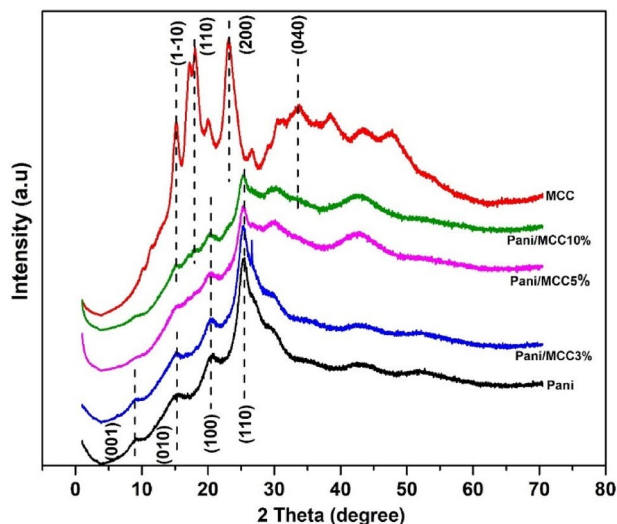


Fig. 1 XRD patterns of Pani, MCC, and Pani/MCC composites

pure Pani mainly with low amount of MCC. In addition, the characteristic peaks at 15.37°, 17.92° and 34.08°2 θ and related to the cellulose component appear as expected and their intensity increase in intensity with increasing the amount of cellulose in the sample increases. As no extra reflections were detected, the presence of peaks characteristic of both components, with no 2 θ shifting, suggests the formation of a new Pani-cellulose composite which can be explained by possible interactions Pani-MCC via hydrogen bonds (Scheme 3).

The average crystallite sizes, D , were estimated from the Scherrer equation (Eq. 2) [66, 67] using the BRUKER AXS software TOPAS 6.0 [68, 69].

All Bragg peaks were fitted with the fundamental parameters approach (FPA). This approach considers both instrumental and micro-structural contributions to the integral breadth, and thus the crystallite size for each Bragg peak could be determined and their mean value was reported.

$$D = \frac{0.98\lambda}{\beta \cos\theta} \quad (2)$$

where D is the crystallite size (nm), λ the wavelength of light (nm), β the full width at half maximum (FWHM) (Rad), and θ is Bragg's angle (Rad) corresponding to the most intense peak (Table 1).

The average crystallite sizes, D decrease for the composites reflecting the low crystallinity compared with those of the parent materials Pani and MCC. This finding can be explained by the fact that the crystal structures of both Pani and MCC are affected after the composite formation.

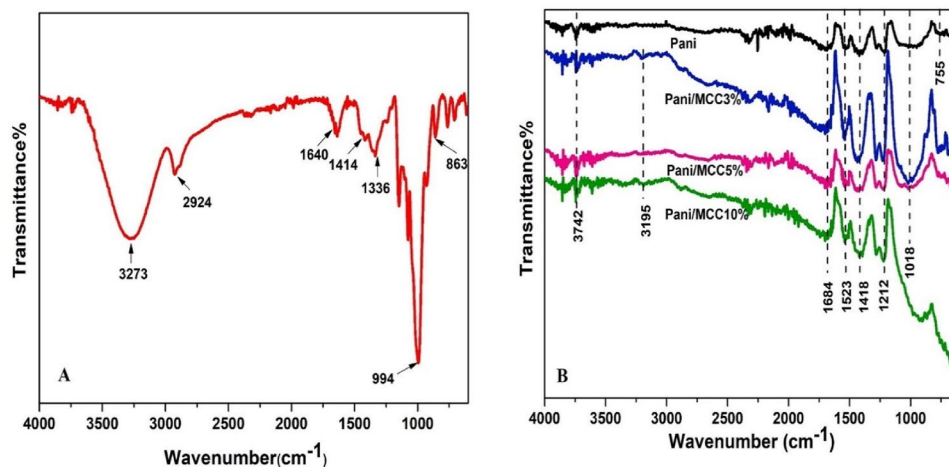
Table 1 D values of Pani, MCC and composites

Sample	Pani	MCC	Pani/MCC3%	Pani/MCC5%	Pani/MCC10%
D (nm)	2.94	2.84	1.66	1.58	1.65

3.1.2 Fourier transform infrared spectroscopy (FTIR)

The FTIR spectra of pure Pani and Pani/MCC 3%,5%,10% are shown in Fig. 2 The pure Pani shows a peak at 755 cm^{-1} corresponding to the out-of plane bending vibration of the C-H aromatic band in the 1,4 disubstituted ring. The 1018 cm^{-1} band is a vibrational mode of B-NH⁺=Q or B-NH⁺-B, which is formed in doping reactions [70]. The peaks at 1418 and 1212 cm^{-1} are due to the stretching of the C-N band and vibration of C-H in the benzene ring. The peaks around 1523 and 1684 cm^{-1} are assigned to stretching vibration of N-B-N and N=Q=N structures, respectively (B and Q represent benzenoid and quinoid moieties in the Pani chains). The peak at 3742 cm^{-1} is attributed to N-H stretching vibration mode of the NH₂ group [71].The FTIR spectra of MCC (Fig. 2) depicts a strong and weak bands at 3273 cm^{-1} and 1640 cm^{-1} respectively originate from the stretching and bending of hydroxyl group in the MCC structure. Whereas, the peak observed in 2924 cm^{-1} due to the asymmetric stretching vibration of CH₂ in pyranoid ring. Indeed, the peak at 1336 cm^{-1} corresponds to the O-H bending of CH₂-OH group. The strong band at 994 cm^{-1} is due to the C-O-C bond of the cyclic alcohol of cellulose [72-75]. In addition to these previous bands, the peaks at 1414-863 cm^{-1} are assigned to CH₂ scissoring in the spectra of cellulose samples (anomeric vibration, specific for β -glucosides), defining them as cellulose I [76]. Furthermore, the FTIR spectra of the Pani/MCC10% composite revealed overlapped adsorption bands of pure Pani and MCC. This fact can be explained by the aniline polymerization on the surface of microcrystalline cellulose. The prepared composites show two peaks around 1523 and 1684 cm^{-1} attributed to stretching vibration of N-B-N and N=Q=N structures, respectively. The peak of hydroxyl stretching shifted from 3273 cm^{-1} to 3195 cm^{-1} with lower intensity, denotes the very strong interaction between the -OH groups of cellulose and NH groups of polyaniline.

Fig. 2 FTIR Spectra of: **A** MCC, **B** Pani, Pani/MCC 3%, 5%, 10% composites



Thus, the band at 1018 cm^{-1} disappears, assigned to the vibration mode of the $-\text{NH}^+$, probably it was hidden by the bands of cellulose in agreement with previous studies [77]. All suggests the presence of the hydrogen bonding interactions between the N–H of the group CH-NH_2 of polymer and O–H bond of MCC. Among the composites, Pani/MCC 10% can be referred as the ideal composite for further investigations.

3.1.3 Textural properties

The argon adsorption/desorption isotherms shapes of Pani and Pani/MCC 10% (Fig. 3A–C) correspond to type IV, characteristic of mesoporous materials [58, 78]. Hysteresis

loops appeared at relatively high pressures of $0.7 P/P_0$. This hysteresis loop was caused by capillary condensation into the pores. On the other hand, MCC exhibits type II isotherm. (Fig. 3B).

Textural parameters including specific surface areas SSA, total pore volume, mesoporous volume V_{mes} , and microporous volume V_{mic} of the prepared materials are summarized in Table 2. The obtained results revealed that MCC exhibits very low SSA and textural features. The composite Pani/MCC 10% presents a SSA almost equal to that of pure Pani. Furthermore, the pore volume of the composite decreased especially in the mesoporous range compared to the pure Pani (Table 2).

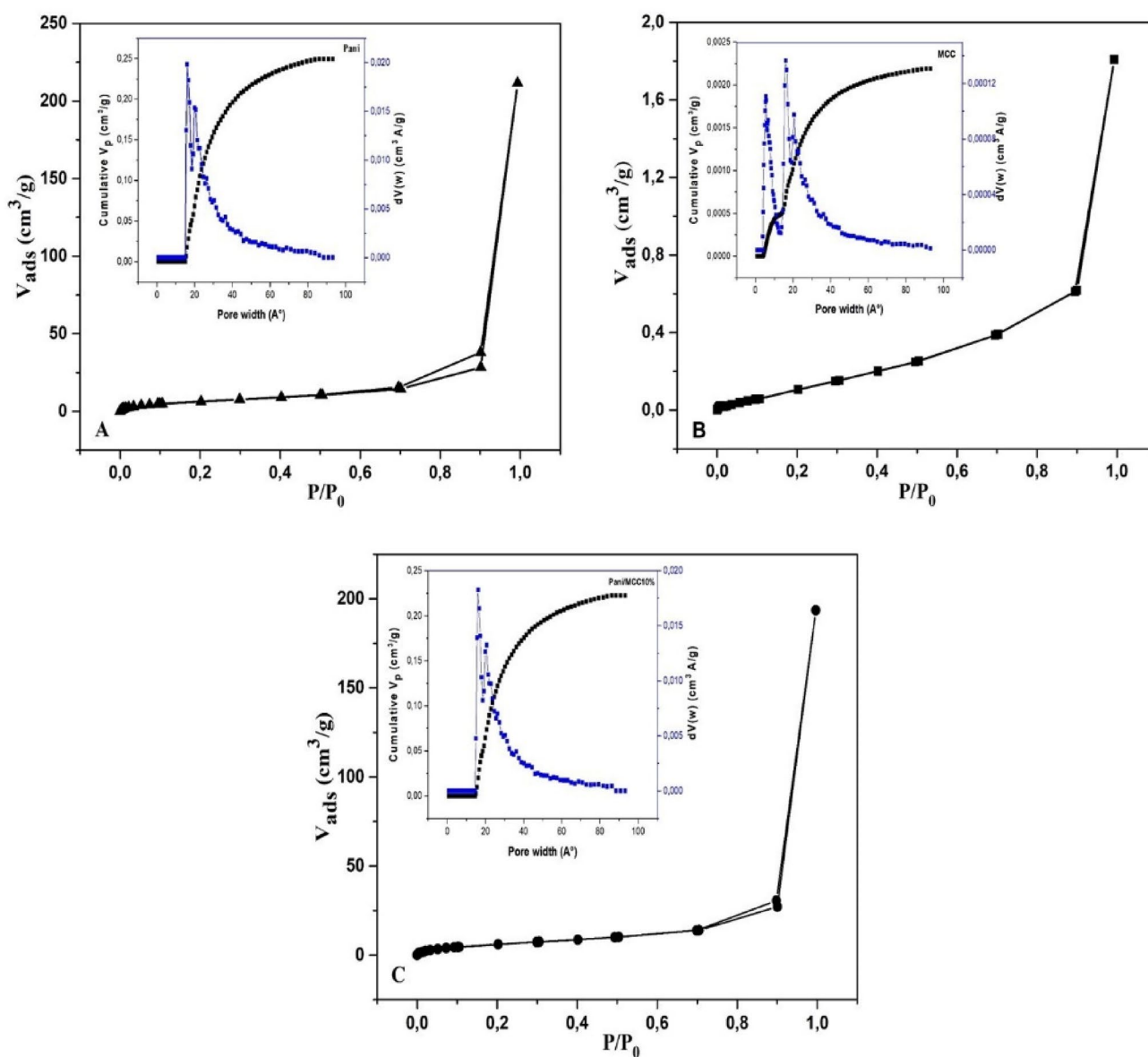


Fig. 3 Argon adsorption–desorption isotherms and inset Pore size distribution of **A** Pani, **B** MCC, **C** Pani/MCC 10%

Table 2 Textural properties of Pani, MCC and Pani-MCC samples

Material	SSA ^a (m ² /g)	V _{PDFT} ^b (cm ³ /g)	V _{mic} ^c (cm ³ /g)	V _{mes} ^d (cm ³ /g)
Pani	22.0	0.2493	0.0686	0.1807
MCC	0.4	0.0022	0.0010	0.0012
Pani/MCC 10%	21.0	0.2226	0.0645	0.1581

^aSpecific surface area^bTotal pore volume^cMicropores volume^dMesopores volume

Figure 3 shows the NLDFT cumulative pore volume as well as the corresponding pore size distribution PSD curves of Pani, MCC and Pani/MCC 10% composite.

For both pure Pani and synthesised composite, the distribution presents a narrow peak centred around 15 Å and a large peak from 20 to 60 Å. The corresponding cumulative pore volume shows the Ar filling in the micro and mesopores range. About Regarding MCC, the distribution shows a narrow peak from 5 to 15 Å, and a peak centred around 15 Å, another large peak from 20 to 60 Å. These results show that the MCC was well dispersed in the mesopores of Pani framework and it is well supported by changes in pore size distribution (Fig. 3).

3.1.4 Thermal analysis

The study of the thermal properties of materials using TGA/DTG is important to investigate the response to a change in temperature. Pani (Fig. 4A) exhibits three major weight loss steps. The first weight loss (10.36%) attributed to the release of physisorbed water that occurred from 56 to 187 °C. The second weight loss (13.70%) between 210 and 320 °C is caused by the dedoping and a gradual decomposition initiated by dopants. Lastly the third stage happened around 370 °C (36, 32%) and is attributed to decomposition of the polymer backbone, the polymer chain breaks down and this can may lead to the production of gases such as acetylene and ammonia [79, 80]. The TGA/DTG curves of MCC (Fig. 4B) show two-step thermal decomposition starting from 30 °C to 150 °C, which corresponds to the moisture removal of the absorbed and intermolecular H-bonded water with weight loss (≈10%) [81]. The majority of the weight loss (≈80%) occur during the second stage around 290 °C attributed to the polymer chain scission, related to the departure of molecular fragments such as O–H and H₂C–OH groups [77]. The TGA curve of Pani/MCC 10% composite (Fig. 4C) shows three degradation steps. The first weight loss (13.15%) observed within 100 °C is attributed to the composite dehydration. The second weight loss (27.92%) is attributed to the pyrolysis of cellulose, its observed over the range from 220 °C to 480 °C. The thermal decomposition of the cellulose content in the Pani/MCC composite occurred at

higher temperature compared to that of pure MCC, indicating that the Pani covered the surface of cellulose [82]. The third weight loss (25.60%) of the Pani/MCC composite was observed from above 500 °C, corresponding to the thermal decomposition of the Pani. The thermal stability of cellulose was noticeably increased by incorporating Pani acting as protective barrier which reduced the thermal decomposition rate [47]. As summary, Pani improved the thermal stability of composite as compared to the pure MCC by degradation of the biopolymer at temperatures higher than 290 °C.

3.1.5 Scanning electron microscopy

The SEM characterization of pure Pani and Pani/MCC are presented in Fig. 5, the pure Pani (Fig. 5A) shows a large particles aggregates, with sizes up to several microns without a defined shape though spherical a fiber-like geometries seem to be predominant as observed at higher magnifications (Fig. 5A) and an agglomerated structure. Images of the MCC (Fig. 5B) clearly show spherical particles size in 5 to 10 micron range with homogeneous surfaces. The morphology of the composite (Fig. 5C) indicates the presence of highly agglomerated structures. This behaviour can be explained by aqueous in situ polymerization of aniline on hydrophilic surface of cellulose. It seems that spherical particles of MCC have been hidden by the polymer chain proving the polymerization of aniline on the cellulose surface. These results are in agreement with the decrease of the pore volume of Pani after MCC coating.

3.2 Transmission electron microscopy

TEM is an adequate technique to observe the shape and size of particles at the nanoscale resolution. TEM micrographs of Pani and Pani/MCC 10% are shown in Fig. 6. As underlined by other researchers [83]. Particles of Pani produced by techniques of oxidative aniline polymerization in an inorganic acid aqueous solution have a high surface tension, resulting in their tendency to aggregate, and a low specific surface leading to large aggregates of Pani particles with sizes up to several microns. The basic units formed during oxidative chemical polymerization of Pani are nanofibers (also visible

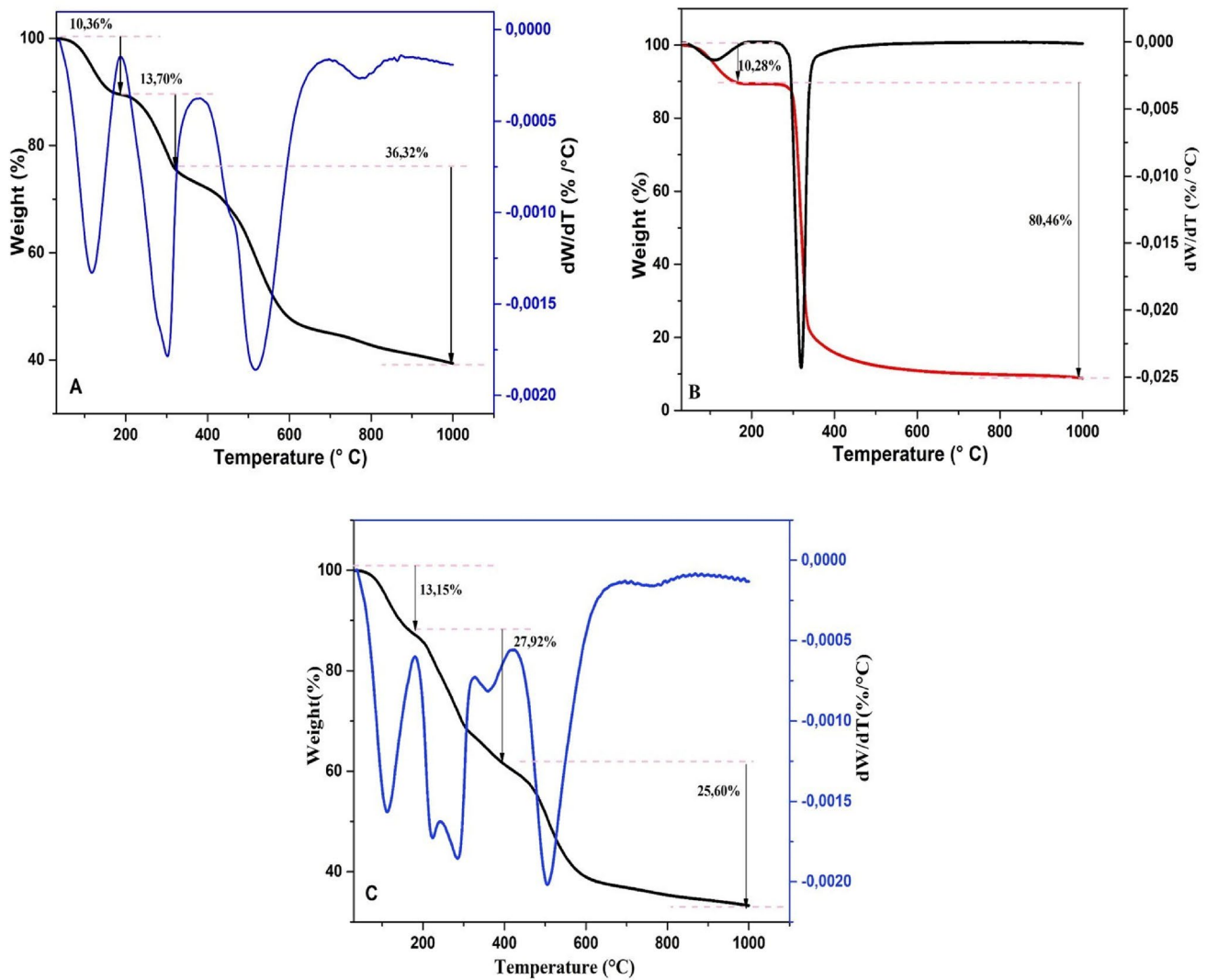


Fig. 4 TGA/DTG analysis curves for; A Pani, B MCC, C Pani/MCC 10% composite

by SEM see Fig. 5) but with the progress of the polymerization, the formed nanofiber will serve as scaffolds for the further growth of Pani and finally develop to a particle form. Thus, non-uniform granular aggregation was observed for pristine Pani due to multilevel irregular secondary growth (Fig. 6A). Nevertheless, smaller particles (< 10 nm) can also be observed in some regions. From Fig. 6B it seems that particles have spherical shape, with very small size (nano range) less than 2 nm and tend prone to form aggregates, due to their large surface area and the interaction between the particles. The particles sizes observed are in good agreement with the values of the crystallites size estimated by XRD. Molecular conformations and rearrangement of polymers within a composite material is greatly influenced by the extent of inter/intra hydrogen bonding. Hydroxyl and carboxylic groups of MCC promote multiple inter/intra hydrogen-bonds, thus increasing the strength and density of the

material as confirmed by the compactness of nanoparticles (aspect of fused surface) and the fiber/rod-like geometries observed by both SEM and TEM.

3.3 Photocatalytic properties

To study the optical properties of the prepared photocatalysts, the UV diffuse reflectance UV-Vis/DR spectra were recorded for the estimation of band gap energy of the photocatalysts using the given below Kubelka-Munk equation:

$$K = \frac{(1 - R)^2}{2R} \quad (3)$$

where **K** is the transformed reflectance and **R** is the reflectance (%).

Fig. 5 SEM micrographs of **A** Pani, **B** MCC, **C** Pani/MCC 10% composite

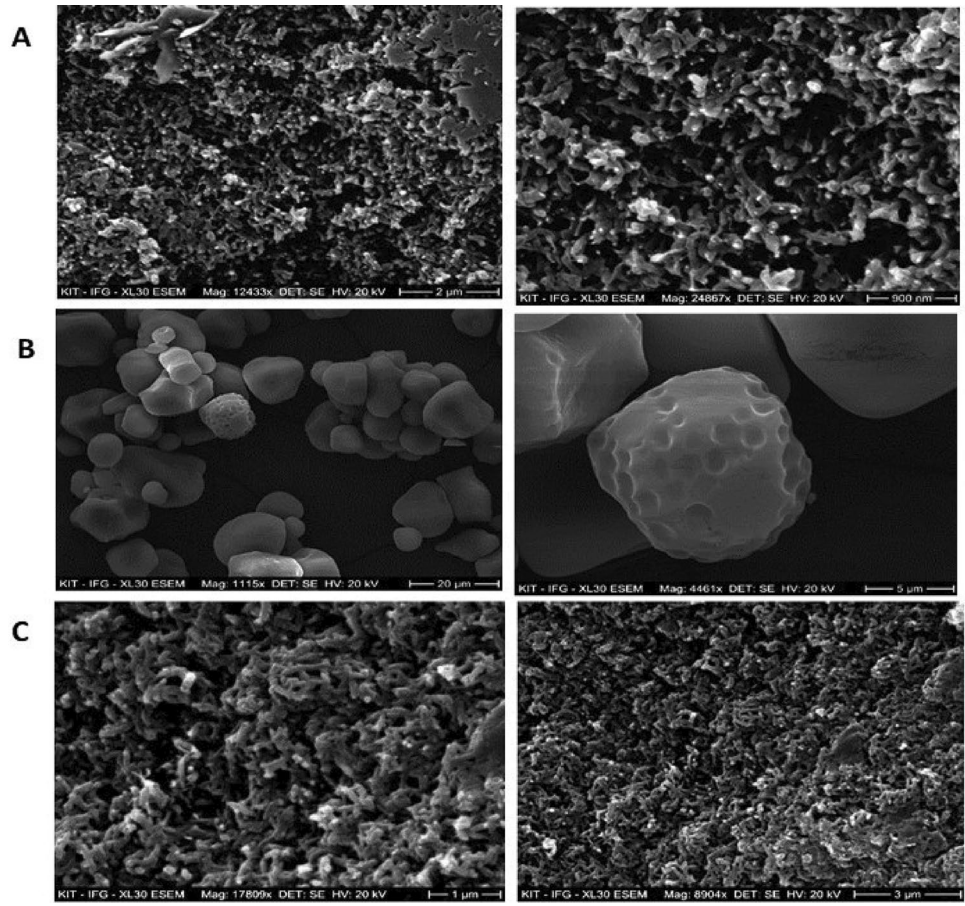
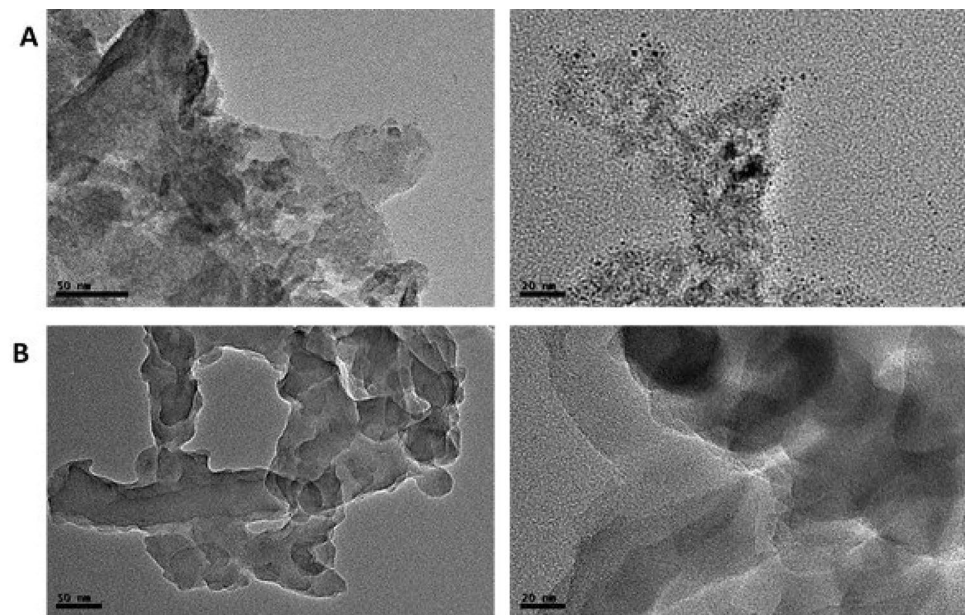


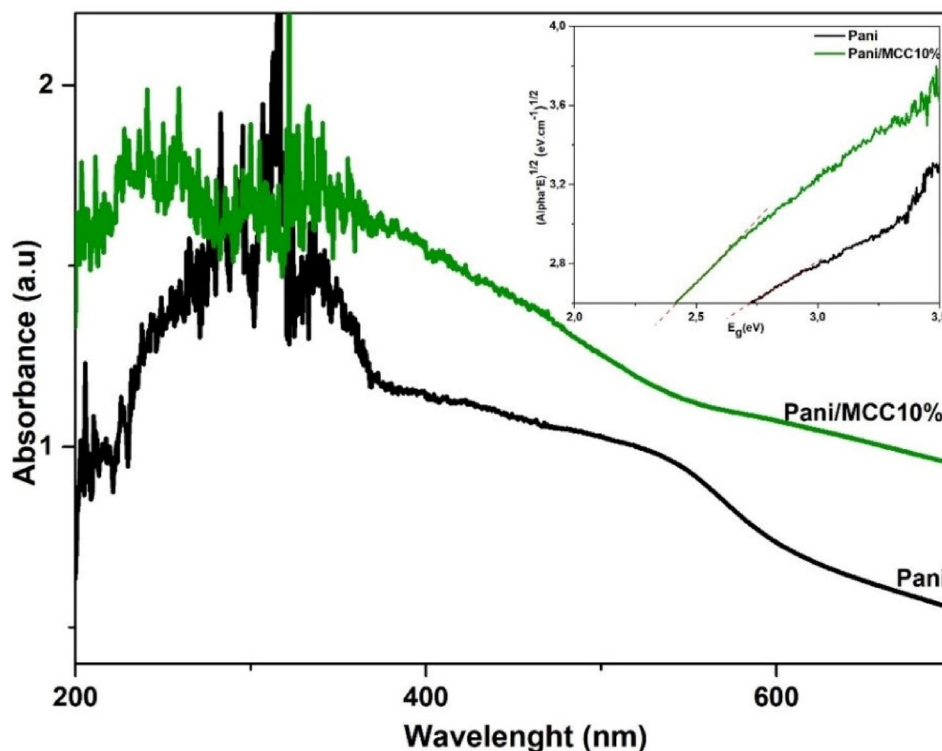
Fig. 6 TEM micrographs of **A** Pani, **B** Pani/MCC 10% composite



The Tauc plots of $(\alpha h \nu)^2$ vs $(h\nu)$ were plotted to calculate the band gap (Fig. 7), where α is the absorption coefficient and $(h\nu)$ is a photon energy. Based on the estimated band gap energies (E_g), the potential positions of the conduction

and valence bands of both Pani and cellulose modified Pani semiconductors were estimated for $n=2$. The values of band gap energies show that the intrinsic absorption band of cellulose modified Pani ($E_g = 2.41$ eV) shifts into infrared region

Fig. 7 UV–vis spectra of Pani and Pani/MCC 10% photocatalysts and evolution of $(\alpha E)^2$ as a function of the energy



in comparison with pure Pani ($E_g = 2.61$ eV). This phenomenon may be due to charge transfer between electrons of Pani/MCC in the systems and means that lower energy is needed for the displacement of electron from BV (band valance) to BC (band of conduction). Therefore, the absorption band of Pani changes with its modification with cellulose. This suggests that Pani/MCC 10% can absorb in UV–visible region.

3.3.1 Photocatalytic degradation of methyl orange

The photocatalytic activities of Pani and the composite based on Pani were evaluated in the photodegradation of MO in aqueous solution under UV–visible light irradiation. The photodegradation of MO, at regular time intervals was followed by light absorption as indicated in the experimental section. As shown in Fig. 8A, in the absence of irradiation, only a slight light absorption was observed (less than 3%). The obtained photodegradation results indicate that both catalyst and light are mandatory for MO photodegradation efficiency. It is worth recalling that the strong absorption band of MO, located at $\lambda = 463$ nm, decreased as the irradiation times increased. The decrease of the absorption of the photocatalysts was indicated by decolorization of MO dye due to decrease of the MO dye concentration. Finally, this band was disappeared within 75 min when Pani/MCC 10% was used as a photocatalyst.

The stability of the photocatalyst was tested to examine the cost-effectiveness of the process. Pani/MCC 10% was

assessed in four consecutive cycles by using fresh dye solution at experimental conditions. It is useful to know that, between each cycle, the photocatalyst was recovered by centrifugation and then washed with deionized water and dried at 80 °C for 4 h and finally reused. As seen from Fig. 8B, a gradual and light decrease in the photoactivity of Pani/MCC 10% was observed, MO photodegradation remained almost unchanged, between 93 and 97% (Fig. 8B).

3.4 Kinetic studies

It was worth recalling that an increase in the concentration of the contaminant involves a decrease in the photocatalytic reaction rate. Generally, the kinetics follows a Langmuir–Hinshelwood mechanism (Eq. 4) confirming the heterogeneous catalytic character [29, 84].

$$r = -\frac{dC}{dt} = \frac{k'KC}{1 + KC} = k'\theta \quad (4)$$

where r is the reaction rate (mg/L min), k' the rate constant of photocatalysis in (mg/L min), K the rate constant of the adsorption (L/mg), C the concentration of dye solution in (mg/L),

C the concentration of dye solution at any time and t the time in (min). The model of L–H supposes that both species are present in a monolayer at the solid liquid interface and control the rate-determining step of the process

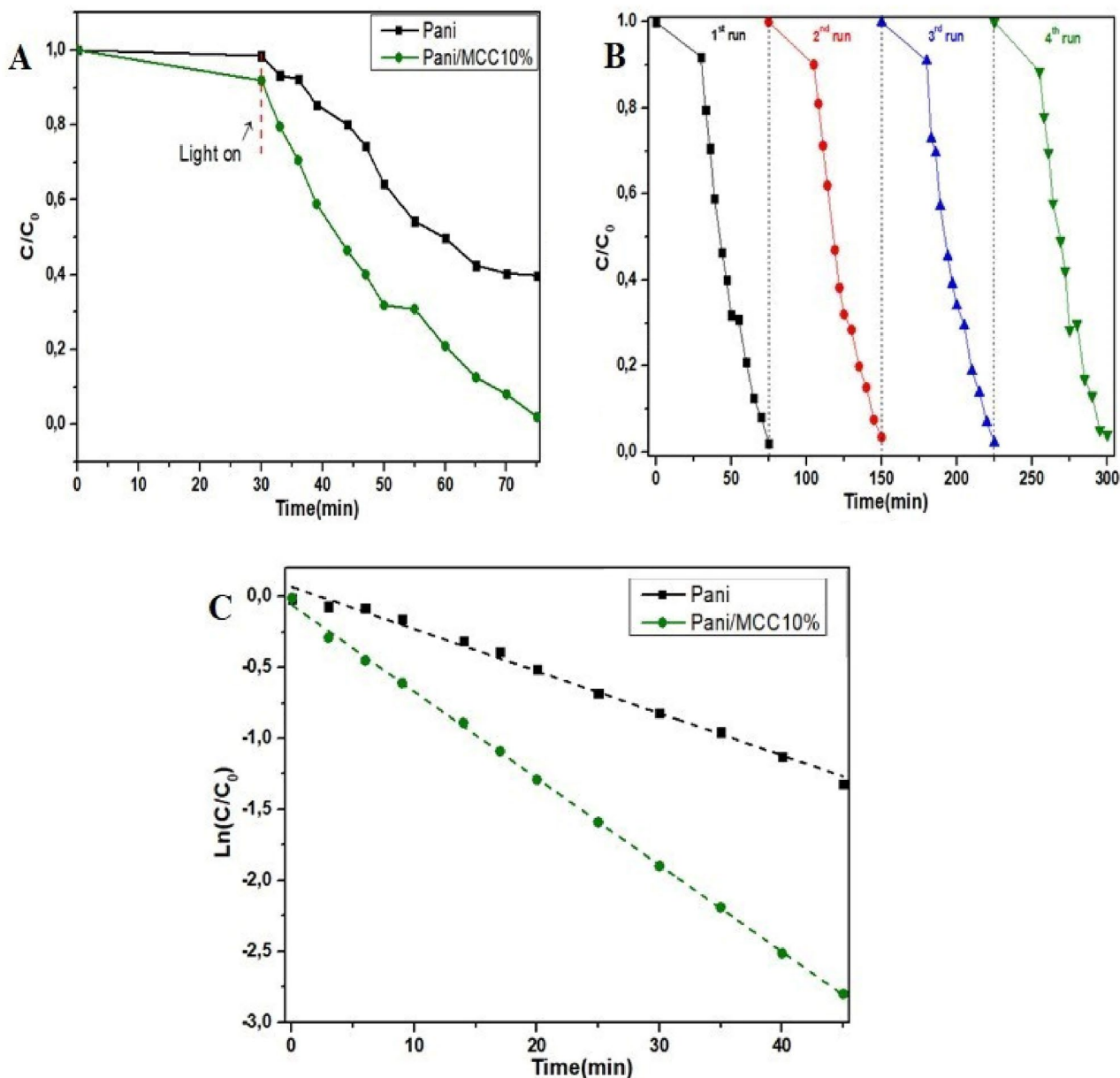


Fig. 8 **A** Photodegradation curves of MO using prepared photocatalysts under UV-Visible irradiation ($\lambda=360$ nm). **B** Stability test result of Pani/MCC 10% photocatalyst after four cycles for photodegradation of MO. **C** pseudo-first order kinetics plots of MO

[85]. The logarithmic form of the Eq. (5) (the integral of Eq. (4) is similar to an apparent first-order equation, where C_0 and C_t are the initial and final concentrations of the pollutant respectively, t is the irradiation time and k shows apparent first-order rate constant [86]. The reaction rate stabilizes and becomes independent of C which gives a zero-order kinetics situation ($r=k_0$, where k_0 is the zero order rate constant). Equation (5) is a zero order at high concentrations ($C > 5$ mM) whereas at concentrations below 1 mM the reaction is considered as an apparent first order reaction.

$$\ln(C_0/C) + k'(C_0 - C_t) = k'Kt = kt \quad (5)$$

At higher concentrations, all the catalytic sites on the catalyst surface are occupied by the adsorbed reactant molecules. For diluted solutions, the reaction rate is proportional to the initial concentration and the reaction is of the apparent first order ($r = -dC/dt = kKC = k_1C$ or $\ln(C_t/C_0) = -k_1t$, where k_1 is a first order rate constant in (min^{-1})). At low concentrations, the number of catalytic sites will not be a limiting factor and the rate of decolorization is proportional to the concentration of the dye [84, 87].

$\ln(C/C_0)$ was plotted as a function of the irradiation time (Fig. 8C) in order to calculate k values. The rate constant values (k (min^{-1})) are calculated from the straight-line portion of the first-order plots summarized in Table 3. The linear correlation between $\ln(C/C_0)$ and irradiation time, suggested that photocatalytic process of MO dye degradation follows the pseudo-first-order reaction kinetics (Eq. 6) [88].

$$\ln(C_0/C_t) = kt \quad (6)$$

The constant of photodegradation rate (k) using Pani/MCC 10% (0.043 min^{-1}) was higher than that of pure Pani (0.020 min^{-1}) (Table 3) which clearly reveals a higher rate of photodegradation using Pani/MCC 10%.

The improvement in photocatalytic activity for Pani/MCC photocatalyst at 10 wt% loading of cellulose can be due to several factors. The modification of Pani with cellulose leads to the formation of Schottky barrier at the interface between Pani semi-conductor and cellulose resulting in an efficient channeling of electrons from the Pani to the novel formed interface (Fig. 6). The decrease in the number of electrons in Pani leads to (e^-/h^+) pair recombination and provides the enhancement of the photocatalytic activity of the catalysts [27, 29]. It was observed that the degradation in the first 30 min was very fast during and after this, it began to slow down. The ultimate degradation of MO was found beyond 97% for MO during the investigated reaction time of 70 min. When Pani and its composite were illuminated with UV light, it absorbs photons to generate electron-hole pairs due to the $\pi-\pi^*$ transition occurring in Pani, and these pairs generate the hydroxyl radicals (OH^\bullet) by reacting with water molecules [89, 90]. The degradation goes to maximum till 30 min, which is due to the availability of O_2 and initially more OH^\bullet radicals generated rapidly, thus a large number of photons reaching the catalyst surface [91]. One more reason for the fast initial rate of degradation in the first 30 min is the presence of the pores on the surface of the composite, as shown in the SEM, TEM images and the Ar adsorption analysis (Table 2), which act as active sites to adsorb the dyes molecule [92]. These adsorbed molecules are captured by photogenerated oxidizing species (OH^\bullet) and degraded immediately. The availability of these active sites decreased leading to the decrease of the oxidizing species (OH^\bullet) as well as the degradation rate [92, 93]. Indeed, the catalytic activity

Table 3 The degradation rates, constant rate (k), half-lives ($T_{1/2}$), and coefficients of determination (R^2) for the MO photodegradation with different photocatalysts

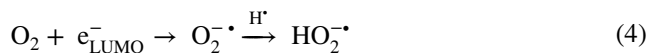
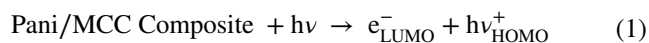
Photocatalyst	Degradation rate (%)	Rate constant (k , min^{-1})	Half-lives ($T_{1/2}$, min)	R^2
Pani	43.22	0.020	34.65	0.9633
Pani/MCC10%	62.12	0.043	16.11	0.9858

instead decreased sharply because of the fact that excessive Pani acts as the electron-hole recombination center [94]. Meanwhile, the photodegradation of anionic dyes is promoted by adsorption due to the interaction between the negatively charged groups and the positively charged backbone of Pani [95]. Thereby, the newly formed polaron band in Pani-ES has a greater number of delocalized electrons, which can facilitate electron transfer and thus improve the photoactivity [96]. In addition, the electron transfer in Pani-ES can be improved by homogenous and composite high surface area as revealed by the SEM and SSA results.

The photocatalytic performance of the present composite is compared with other reported composites as illustrated in Table 4. A photocatalytic degradation of 97% has been found within 70 min for 30 ppm MO solution. Thus, the present composite offers enhanced photodegradation under UV-visible light.

3.4.1 Proposed photocatalytic mechanism

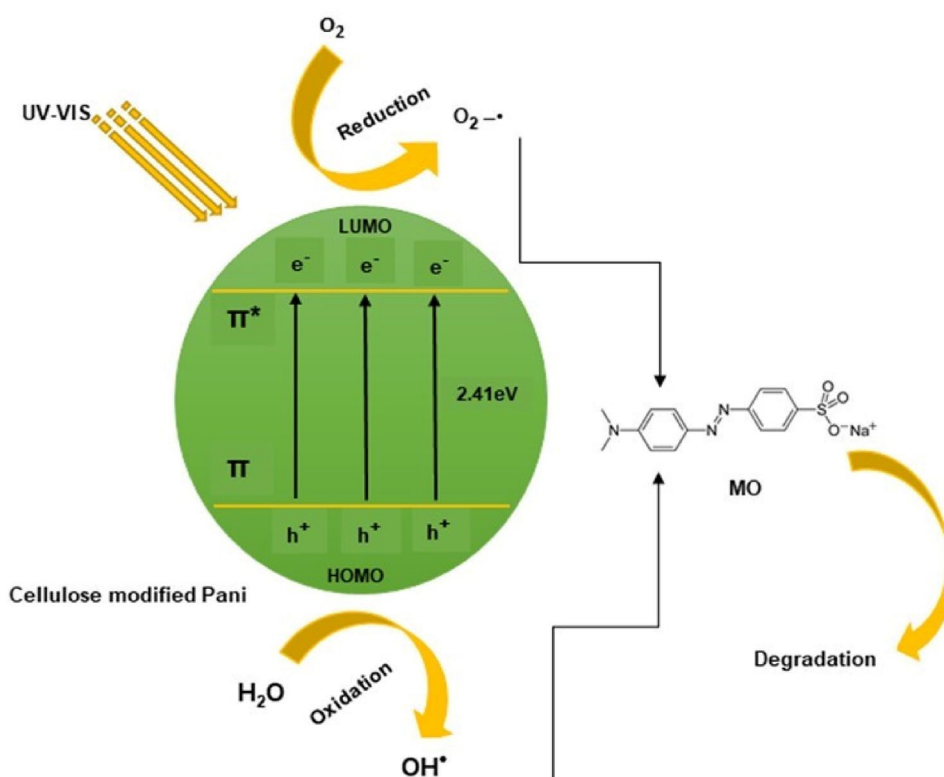
The possible involved mechanism in the photodegradation of Pani/MCC10% has been proposed (Fig. 9) and it is shown in the following reactions:



The holes created in the valence band (HOMO) form hydroxyl radicals (OH^\bullet) via the oxidative reactions (Reaction 2). Therefore, the electrons in the LUMO form super oxide radical anions ($\text{O}_2^{\bullet -}$) through the reductive reactions (Reactions 3, 4). It is worth noting that the two radicals OH^\bullet and $\text{O}_2^{\bullet -}$ are strong oxidants that can oxidize the organic compounds. Emphasizing that $\text{O}_2^{\bullet -}$ has a sufficient reduction potential that allows oxidizing organic species with strong electron-donating groups (such as active azo $-\text{N}=\text{N}-$ bond); however, radical OH^\bullet tends to remove hydrogen or attack the C-C unsaturated bonds [48, 105, 106]. Hence, a model pollutant containing unsaturated C-C bonds such as MO can probably be photocatalytically oxidized with OH^\bullet radicals formed.

Table 4 Applications of Pani Composites in the photodegradation of organic molecules from the literature

Photocatalyst	Pollutant	Degradation efficiency %	Eg (eV)	Reaction conditions	Ref
Pani/TiO ₂ /rGH	B.P.A	80	2.45	40 mn, 40 ppm	[97]
Ag ₃ PO ₄ /Pani	Phenol/2,4-dichloro phenol	100–34.6	/	30 mn, Visible light, 10 ppm	[98]
BiVO ₄ /Ag ₃ PO ₄ /Pani	CIP (antibacterial agent)	85.92	/	60 mn, Visible light, 10 ppm	[99]
Pani/ZnO ₂	OM/MB	69.8/74.6		180 mn, Visible light	[100]
Pani/ZnO ₂ 1.5		98.3/99.2	2.67		
Pani/ZnO ₂ 2		24.7/39.7	2.59		
Pani/BiVO ₄	Rhodamin B Phenol		2.29	60 mn, Visible light 120 mn, Visible light, 20 mg/l	[101]
Pani/PbS	Rhodamin 6G	87	/	50 mn, Visible light, 20 ppm	[102]
Pani/ZnO	Acid blue	90	/	60 mn, Solar irradiation, 30 ppm	[103]
Pani/TiO ₂	Methylene blue	99.6	/	60 mn, Visible light, 10 ppm	[104]
	RhB	95.6		30 mn	
Pani/decorated cellulose aerogel	Methylene blue	95	/	20 mn, Natural sunlight, 20 ppm	[47]
		60		120 mn, Visible light	
Pani/MCC	MO	97	2.61	70 mn, UV–vis light, 30 ppm	This work

Fig. 9 Proposed pathway for MO photodegradation using Cellulose modified Pani under UV–vis irradiation

4 Conclusion

The Pani/MCC composite was successfully prepared using in situ polymerization of aniline in the presence of MCC by addition of APS as oxidant. The obtained composite was evaluated as photocatalyst for degradation of anionic

dyes from aqueous solutions. The characterization techniques reveal that the conductive polymer was perfectly immobilized perfectly in the biopolymer framework. Furthermore, the formed composite results from Pani-MCC interactions between NH-Pani and OH-MCC groups in the mesoporous surface of Pani revealed by BET and PSD. SEM and TEM confirmed good dispersion of MCC in the

Pani sample. It was observed that Pani/MCC10% showed a high degradation capacity for anionic dye reaching 97%. The R^2 value showed that, the degradation process of dyes on the composite followed first order kinetics, suggesting that the removal mechanism can be related to the interactions between NH_2 and OH functional groups on the composite with anionic MO dye is provided by electrostatic attractions forces.

The photocatalytic activity was found to depend strongly on the structure, catalyst type, and specific surface area of the catalyst. The polymer conductivity increases the electron delocalization, which can facilitate electron transfer and improve the photoactivity. MCC increased the dispersibility of Pani particles in aqueous solution, which resulted in better catalytic activity. The presence of the pores on the composite surface, acts as active sites to adsorb the dyes molecules. Moreover, this catalyst was very stable after three cycles of reuse and efficient under UV-Vis. Therefore, it is of much interest as a potential catalyst for the treatment of wastewater under UV-Vis.

Acknowledgements S.N. Benaouda is grateful to the Erasmus+KA107 project for the doctoral mobility. S.N. Benaouda thanks Prof. Driss Nehari, Dr. Kamel Demmouche and Dr. Abdelkader Nebatti (Ain Temouchent University, Algeria) for their precious help in the Erasmus application. The authors are grateful to the reviewers for their constructive comments and corrections that improved the manuscript.

Author's contribution SNB, HC: Material preparation, data collection, Investigation, analysis, and writing; FA: Investigation and Methodology, CB: Supervision, Investigation and Methodology; HT, PGW: Investigation and Methodology; AB: Supervision, analysis; JCV: Investigation and Methodology; RH: Analysis, Validation, Supervision.

Declarations

Competing interest The authors have no conflicts of interest to declare that are relevant to the content of this article.

References

- S.J. Eichhorn, A. Gandini, G. Editors, *MRS Bull.* **35**, 187 (2010)
- F. Galembek et al., *Acad. Bras. Cienc.* (2019). <https://doi.org/10.1590/0001-3765201920181160>
- M. Bahrami, J. Abenojar, M.A. Martinez, *Mater.* **13**, 1545 (2020)
- J. Li, X. Qu, L. Wang, X. An, *BioResour.* **5**, 712 (2010)
- J. Jin, Y. Su, Y. Duan, *Sens. Actu. B Chem.* **72**, 75 (2001)
- M.V. Kulkarni, A.K. Viswanath, *Sens. Actu. B Chem.* **107**, 791 (2005)
- P. Kong, N. Chen, Y. Lu, S. Li, P. Wang, *RSC Adv.* **9**, 9211 (2019)
- A. Kumar, V. Kumar, K. Awasthi, *Polym. Plast. Technol. Eng.* **57**, 70 (2018)
- A. Hsini et al., *J. Mol. Liq.* **316**, 113832 (2020)
- A. Hsini et al., *J. Coll. Interf. Sci.* **585**, 560 (2021)
- A. Hsini et al., *Coll. Surf., A* **617**, 126274 (2021)
- A. Hsini et al., *J. Environ. Chem. Eng.* **9**, 105885 (2021)
- M. Laabd et al., *J. Hazard. Mater.* **422**, 126857 (2022)
- A. Imgharn et al., *Chem. Phys. Lett.* **778**, 138811 (2021)
- L. Brini et al., *Water Sci. Technol.* **84**, 2265 (2021)
- L. Brini et al., *Int. J. Environ. Anal. Chem.* **2021**, 1 (2021)
- A. Imgharn et al., *Chemosphere* **295**, 133786 (2022)
- A. Hsini et al., *RSC Adv.* **11**, 31272 (2021)
- S. Bhadra et al., *Prog. Polym. Sci.* **34**, 783 (2009)
- M. Gvozdenovic et al., *Hemijska Indust.* **68**, 673 (2014)
- T.S. Najim, A.J. Salim, *Arab. J. Chem.* **10**, 3459 (2017)
- D. Trache et al., *Int J Biol Macromol.* **93**, 789 (2016)
- D. Trache, *Handbook of composites from renewable materials* (Wiley, 2017)
- E. Shakir, Z. Zahraw, A.H.M.J. Al-Obaidy, *Egypt. J. Pet.* **26**, 95 (2017)
- X. Xia et al., *Front Chem.* **8**, 592056 (2020)
- R.S. Shinde et al., *J. Inorg. Organomet. Polym Mater.* **32**, 1045 (2022)
- H. Chaker et al., *Chem. Eng. Res. Des.* **171**, 198 (2021)
- H. Chaker et al., *J. Environ. Chem. Eng.* **9**, 104584 (2021)
- H. Chaker et al., *ChemistrySelect* **5**, 11787 (2020)
- Y. Naciri et al., *J. Coll. Interf. Sci.* **572**, 269 (2020)
- Y. Naciri et al., *Adv. Coll. Interf. Sci.* **280**, 102160 (2020)
- Y. Naciri et al., *Mater. Today: Proc.* **22**, 48 (2020)
- D. Bahnemann, *Sol. Energy* **77**, 445 (2004)
- S.D. Khairnar, V.S. Shrivastava, *J. Taibah Univ. Sci.* **13**, 1108 (2019)
- S.D. Khairnar, M.R. Patil, V.S. Shrivastava, *Iran. J. Catal.* **8**, 143 (2018)
- Y. Naciri et al., *J. Environ. Chem. Eng.* **7**, 103075 (2019)
- A. Shaim et al., *Mediterranean J. Chem.* **8**, 66 (2019)
- Y. Naciri et al., *J. Environ. Chem. Eng.* **6**, 1840 (2018)
- A. Chennah et al., *Mediterranean J. Chem.* **6**, 255 (2018)
- Y. Fahoul et al., *J. Mol. Struct.* **1253**, 132298 (2022)
- K. Tanji et al., *J. Iran. Chem. Soc.* **19**, 1 (2022)
- I. Mimouni et al., *Environ. Sci. Pollut. Res.* **29**, 7984 (2022)
- K. Tanji et al., *React. Kin. Mech. Catal.* **134**, 1017 (2021)
- B. Akhsassi et al., *Chem. Phys. Lett.* **783**, 139046 (2021)
- S. Ferraa et al., *Chem. Phys. Lett.* **763**, 138173 (2021)
- H. Barebita et al., *Solid State Sci.* **108**, 106389 (2020)
- Z. Zhou et al., *RSC Adv.* **4**, 8966 (2014)
- H. Chaker et al., *J. Photochem. Photobiol. A* **318**, 142 (2016)
- L. Zhang, P. Liu, Z. Su, *Polym. Degrad. Stab.* **91**, 2213 (2006)
- S. Yang, X. Song, L. He, F. Liao, *RSC Adv.* **4**, 54810 (2014)
- S. Shahabuddin et al., *Arab. J. Chem.* **11**, 1000 (2018)
- S.S. Sambaza, A. Maity, K. Pillay, *ACS Omega* **5**, 29642 (2020)
- Y. Naciri et al., *Chemosphere* **292**, 133468 (2022)
- S.D. Khairnar et al., *J. Photochem. Photobiol.* **6**, 100030 (2021)
- M.R. Patil, S.D. Khairnar, V. Shrivastava, *Appl. Nanosci.* **6**, 495 (2016)
- S. Brunauer, *Bureau of chemistry* (George Washington University, 1938)
- H. Chaker et al., *Coll. Interf. Sci. Commun.* **43**, 100461 (2021)
- K.S.W. Sing, R.A.W. Haul, L. Moscou, R.A. Pierotti, J. Rouquerol, T. Siemieniewska, *Pure Appl Chem.* **57**, 603 (1985)
- Eddaoudi, M., Particle Technology Series, S. Lowell (Quantachrome Instruments, Boynton Beach), J.E Shields (CW Post Campus of Long Island University), M.A. Thomas, M. Thommes (Quantachrome Instruments) ed, Dordrecht, The Netherlands, (2005).
- J.P. Pouget et al., *Macromolecules* **24**, 779 (1991)
- M. Ayad, G. El-Hefnawy, S. Zaghlol, *Chem. Eng. J.* **217**, 460 (2013)
- B. Boukoussa et al., *J. CO2 Utilizat.* **26**, 171 (2018)
- B. Kondawar, M.D. Deshpande, S.P. Agrawal, *Int. J. Comp. Mater.* **2**, 32 (2012)
- B.H. Lee, H.J. Kim, H.S. Yang, *Curr. Appl. Phys.* **12**, 75 (2012)

65. M.M. Abdi et al., *Molecules*, **23**, 1 (2018)
66. R. Jenkins, R.L. Snyder, *Introduction to X-ray powder diffraction* (Wiley Online Library, 1996)
67. S.D. Khairnar, V.S. Shrivastava, *SN Appl. Sci.* **1**, 1 (2019)
68. A. Coelho, *Topas academic: general profile and structure analysis software for powder diffraction data* (Bruker AXS, Karlsruhe, 2007)
69. R.W. Cheary, A. Coelho, A fundamental parameters approach to X-ray line-profile fitting. *J. Appl. Crystallogr.* **25**, 109 (1992)
70. E.A. Sanches et al., *J. Nanomater.* **2011**, 1 (2011)
71. M. Trchová, J. Stejskal, *Pure Appl. Chem.* **83**, 1803 (2011)
72. M.M. Abdi et al., *AIP Conf. Proc.* **1901**, 100018 (2017)
73. M. KacEuraÁkova, V. Sasinkova, N. Wellner, A. Ebringerova, *Carbohydr. Polym.* **43**, 195 (2000)
74. B.V. Mohite, S.V. Patil, *Phys. Carbohydr Polym.* **106**, 132 (2014)
75. N.D. Tissera et al., *Carbohydr Polym.* **186**, 35 (2018)
76. W.N. Goh, A. Rosma, B. Kaur, A. Fazilah, A.A. Karim, R. Bhat, *Int. Food Res. J.* **19**, 153 (2012)
77. O. Hajlaoui et al., *Chem. Africa.* **3**, 783 (2020)
78. F. Hamidi et al., *Res. Chem. Intermed.* **47**, 4443 (2021)
79. X. Zhang et al., *Polymer* **53**, 2109 (2012)
80. M.J.R. Cardoso, D.M. Lenz, *Mater. Res.* **10**, 425 (2007)
81. A. Kumar et al., *J. Mater. Phys. Chem.* **2**, 1 (2020)
82. R.L. Razalli, P.M. Tahir, A. Moradbak, Y. Sulaiman, L.Y. Heng, *RSC Adv.* **7**, 25191 (2017)
83. U.M. Casado, M.I. Aranguren, N.E. Marcovich, *Ultrason Sonochem.* **21**, 1641 (2014)
84. A. Nezamzadeh-Ejhieh, Z. Salimi, *Appl. Catal. A* **390**, 110 (2010)
85. N. Pourshirband, A. Nezamzadeh-Ejhieh, S.N. Mirsattari, *Spectrochim Acta A Mol Biomol Spectrosc.* **248**, 119110 (2021)
86. N. Omrani, A. Nezamzadeh-Ejhieh, M. Alizadeh, *Desalin. Water Treat.* **162**, 290 (2019)
87. M. Pera-Titus et al., *Appl. Catal. B* **47**, 219 (2004)
88. S.D. Khairnar et al., *SN Appl. Sci.* **2**, 1 (2020)
89. L.L.Y. Manfei, W. Xiangliang, C. Xinlei, S. Yan, Y. Yinkun, H. Yongjun, C. Kesheng, M. Wei, Q. Guang, *RSC Adv.* **9**, 40694 (2019)
90. S. Saha et al., *SN Appl. Sci.* **2**, 6 (2020)
91. M.M. Zahorny et al., *J. Nano. Electron. Phys.* **13**, 05034 (2021)
92. M. Aamir et al., *Desalin. Water Treat.* **57**, 12168 (2015)
93. H. Mittal, M. Khanuja, *Dyes Pigm.* **175**, 108109 (2020)
94. L. Wang et al., *J. Mater. Res.* **35**, 1316 (2020)
95. Y. Liu et al., *Polymers (Basel).* **12**, 1 (2020)
96. P. Kong et al., *Catal. Sci. Technol.* **9**, 753 (2019)
97. F. Chen et al., *Appl. Surf. Sci.* **427**, 123 (2018)
98. L. Liu et al., *Appl. Catal. B* **201**, 92 (2017)
99. S. Chen et al., *Chem. Eng. J.* **382**, 122840 (2020)
100. R. Saravanan et al., *J. Mol. Liq.* **221**, 1029 (2016)
101. M. Shang, S. Sun, J. Ren, L. Zhou, L. Zhang, *Phys. Chem.* **113**, 20228 (2009)
102. V.A. Chhabra et al., *Environ. Res.* **186**, 109615 (2020)
103. V. Gilja et al., *Polymers (Basel).* **10**, 9 (2018)
104. H. Zhang, J. Zhao, Y. Zhu, *Environ. Sci. Technol.* **42**, 3803 (2008)
105. S. Khaoulani et al., *C. R. Chim.* **18**, 23 (2015)
106. S. Salesi, A. Nezamzadeh-Ejhieh, *Environ. Sci. Pollut. Res.* **2022**, 1 (2022)